In C. L. Luengo Hendriks, G. Borgefors, R. Strand, eds., Mathematical Morphology and its Applications to Image and Signal Processing, Lecture Notes in Computer Science, vol. 7883, pp. 508–519,

Automated Quality Inspection of Microfluidic Chips Using Morphologic Techniques

Thomas Schwarzbauer[1,2], Martin Welk[2], and Chris Mayrhofer[1] and Rainer Schubert[2]

[1] Sony DADC Austria, Sonystrasse 20, 5081 Anif/Salzburg, Austria
{thomas.schwarzbauer, chris.mayrhofer}@sonydadc.com
[2] University for Health Sciences, Medical Informatics and Technology (UMIT), Eduard-Wallnöfer-Zentrum 1, 6060 Hall/Tyrol, Austria
{thomas.schwarzbauer, martin.welk, rainer.schubert}@umit.at

Abstract. We apply morphological image processing for quality inspection of microfluidic chips. Based on a comparison of measured topographies with design data, we provide a coherent solution to four central tasks in the quality assessment of injection moulded polymer devices: determination of channel depth, identification of burrs, calculation of transcription accuracy, and detection of defective regions. Experimental comparison to manual quality inspection procedures demonstrates the good performance of the proposed automated method, and reveals its clear advantages in terms of objectivity and reliability.

1 Introduction

Visual quality inspection of industrial products has been an important application field for image processing from its beginnings, see e.g. [15, 24]. Manual quality inspection by humans faces numerous problems [14]. For example, human experts require training and their skills take a lot of time to develop. Even between well-trained individuals, results tend to be observer-dependent. Furthermore, the inspection task can be tedious and difficult. As [15] points out, this conventional kind of quality control is not only slow and costly, but also leads to high scrap rates and does not assure high quality.

In many mass production manufacturing facilities the actual goal is a 100 % quality assurance [15] which is often unfeasible in a manual inspection setting. Hence, there is an ever-increasing demand for automated visual quality inspection.

In this paper, we are concerned with the development of methods for semi-automated quality inspection of microfluidic chips. Being used e.g. for in-vitro diagnostics, life sciences research and medical technology, these chips constitute a rapidly growing market. A microfluidic chip is a polymer plate incorporating channels and filters through which liquid or emulsions can propagate and are led to well-defined compartments where reactions can take place. Channel cross-sections typically measure some tens of micrometers, while filter structures go down to few micrometers in size. For an example, see Fig. 1.

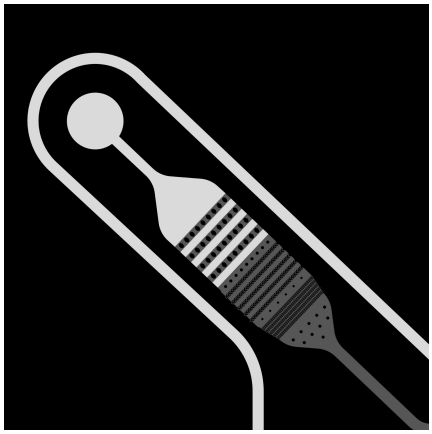

Fig. 1. Detail from a microfluidic chip (design data) featuring channel and filter structures. Grey-values represent depth values on a scale that spreads about 60 µm.

A typical production process involves injection moulding of a half-product plate with open channels and filter structures embossed in its surface, which is afterwards covered by an unstructured even plate. The inspection of the half-product surface is in the focus of our work.

Quality requirements for these products are extremely high due to the fact that they are often used for the processing of unique and sensitive probes. It is of utmost importance to ensure that no probes are wasted due to malfunctions of the chip, and that results of analysis have a high degree of reliability. As a consequence, a thorough quality inspection – ideally, a 100 % quality check – is crucial. At the same time, in order to keep scrap rates low, chips should be discarded only if they feature defects which indeed impair the function of the appliance.

Reviewing quality inspection of surfaces across industries, [24] classifies inspection methods with regard to the underlying features: statistical, structural, filter-based and model-based.

Statistical approaches [24] utilize the spatial distribution of intensity values in images. A variety of statistical features are available and applied in literature for visual inspection. These techniques comprise approaches like histogram statistics, e.g. Ng [16] using global thresholding by Otsu [18], co-occurrence matrices, e.g. Asha et al. [1], Novak and Hocenski [17], as well as registration-based techniques, e.g. Chiou and Zhang [2], Tait et al. [20], Ibrahim et al. [8] and Leta et al. [9].

Structural approaches [24] use texture primitives and their spatial arrangement to analyze images [22]. Apart from primitive measurement, edge features and skeleton representation, also morphological operations are widely used for quality inspection purposes [24]. Elbehiery et al. [4] applied morphological techniques for ceramic tile inspection. Different defects, like chips, cracks or scratches can be detected by applying the proposed approaches, which are all sequences of different image processing techniques, like edge detection, noise reduction and morphology operations. To improve the capability of a morphological approach,

Zheng et al. [26] tried to identify defects on aluminum surfaces by applying genetic algorithms in order to estimate the optimal morphological parameters, a segmentation threshold and a noise reduction threshold. Structural approaches based on morphology are also applied in steel quality inspection by Wiltschi et al. [23].

Filter-based techniques [24] are characterized by the application of filter banks and the computation of the energy of the filter responses. Methods in this category can be divided into techniques applied in spatial domain, frequency domain and joint spatial-frequency domain. Gabor filters were applied by Tsai et al. [21] to detect defects on tile, wood and fabric surfaces. A similar approach was proposed by Lin et al. [11]. They identified defects on optical lenses.

Model-based approaches [24] comprise fractal models [12], random field models [10] or texem models [25].

Our contribution. We describe a system for the inspection of the surface quality of microfluidic chips. It is based on the comparison of topographic data obtained by confocal microscopy to a reference dataset derived from the design model. With a registration step as preprocessing, morphological techniques in combination with segmentation steps provide the core functionality of defect detection, which is in the focus of the present paper. Morphological operations serve as an efficient tool e.g. for noise reduction, recognition of structures and elimination of biasing areas.

Relying on well-established image processing techniques, the contribution of this work is to combine these methodologies into a coherent concept that goes all the way down from the specification of the particular quality inspection task to a practically usable solution.

2 Prerequisites

2.1 Data Acquisition and Problem Statement

In order to assess the conformity of the chip under inspection with its design, the chip is imaged by a confocal microscope at a resolution around 1 µm. This resolution is necessary in order to resolve the finest filter structures on the chip. From the measured data, a topographic map of the chip surface is created. This depth map can be treated as a 2D greyscale image. By design, channel and filter structures on the chip occur in a few discrete depth steps – besides the overall surface level, typically two to three different depth levels are involved.

Given the high resolution, measurement of the entire chip surface is precluded by both storage demand and measurement time. For this reason, the process is applied to regions of interest where critical channel and filter structures are located.

The processing is done by a combination of statistical and structural methods. In order to enable comparison between measured data and the design dataset, both images will have to be aligned. This task is known in image processing as image registration.

Using mainly morphological techniques, the depth map data is then evaluated with regard to several predefined quality criteria. Characteristics like channel depth, accuracy of transcription, and burr are of central interest here. Accuracy of transcription is meant to describe particularly how well filter structures are moulded. Filters typically consist of arrays of pillars, and it is important that these columns reach the overall surface level in order to get in touch with the closing plate. So the main criterion of transcription is the height of the columns. Burrs are raised regions adjacent to channel edges caused by material accumulations after injection moulding. A special challenge here is to discriminate between real burrs and artifacts of the confocal microscope scanning procedure. Transcription accuracy and burrs are indicators for possible functional problems of the chip.

Morphological techniques lend themselves as an excellent tool for the evaluation step because they do not only provide direct solutions to most of the shape processing tasks that occur herein, but also because of their simplicity and speed, which is crucial in view of the large amounts of data that need to be processed. Due to the layered design of the chips, set-valued morphological operations are suitable for our purposes.

2.2 Image Registration

Image registration denotes the task to establish a spatial transformation between the domains of two images by which corresponding points in both images are taken to the same locations. [5] For this to make sense it is understood that both images represent the same scene and differ by time of capture, viewpoint, and/or image modality [27]. Registration problems occur in multiple variations differing e.g. by dimensionality, registration basis, the realm of admissible transformations; registration algorithms differ further in their optimization procedures, and degree of interactivity [13].

In terms of these criteria, the registration problem we face can be described as 2D/2D because the depth dimension in both datasets is treated as (grey-) value. The transformation can be assumed as rigid because the main source of misalignment is the positioning of the probe under the confocal microscope which may be shifted, rotated and tilted, while it is not expected that deformations like shearing or bending of the chip itself as compared to its design model will be large enough to be observable as nonrigid within a region of interest as handled in the registration step. Furthermore, our registration problem is global (with regard to the region of interest), and automatic.

Image registration is nowadays a well-studied problem, and algorithms for a large variety of settings are available.

2.3 Morphology

Once the datasets are aligned, our further processing uses the standard operations of set-valued morphology, see e.g. [6], namely erosion $\ominus$, dilation $\oplus$, opening

$\circ$ and morphological gradient ϱ_B with a structure element B as given by

$$A \ominus B = \{z \in E \mid B_z \subseteq A\} , \tag{1}$$
$$A \oplus B = \{z \in E \mid B_z \cap A \neq 0\} , \tag{2}$$
$$A \circ B = (A \ominus B) \oplus B , \tag{3}$$
$$\varrho_B(A) = (A \oplus B) \setminus (A \ominus B) , \tag{4}$$

where B_z denotes the translate of B to the location z.

2.4 Otsu Segmentation

Otsu segmentation [18] is a threshold-based segmentation method with automatic adaptation of thresholds to the image histogram. In the simplest case of a two-class (e.g. foreground-background) segmentation, a single threshold is chosen such that the ratio $\sigma^2_{\text{inter}}/\sigma^2_{\text{within}}$ of the variance σ^2_{inter} between classes and the variance σ^2_{within} within classes becomes maximal. Given the histogram, the threshold can be computed by an exhaustive search. The method is easily extended to more than two classes by selecting two or more thresholds; however, the cost of exhaustive search increases exponentially with the number of thresholds.

3 Methodology

In the registration step, the design depth-map is kept fixed, and the measured dataset is subject to a rigid transformation. This distribution of roles ensures that structures to be analysed later on are always found at the same positions. The transformation is determined such as to minimize the L_2-distance [3] of the gradient magnitudes between the fixed and transformed images. To this end, we apply a rigid multiresolution approach, see e.g. [5]. It is important here to work with gradients since absolute grey-values – i.e. depths – are affected by slight tilts of the chip caused by bending of the chip, or of the injection moulding mask. Another reason is that the chip can lie askew during the image acquisition due to dust particles on the locating surface. In order to remove this phenomenon from the raw data, the upper surface has to be estimated and subtracted using least squares plane fit [7].

Afterwards, the quality of the chip can be assessed by determining channel depths, identifying burrs, calculating transcription and detecting defects.

3.1 Determination of Channel Depth

The algorithm for determining the global mean channel depth is roughly divided into three steps. The results of the steps are depicted in Fig. 2.

In a first step, the different layers have to be identified. To this end, Otsu segmentation is applied to the corresponding region in the reference image. This

Fig. 2. The results of the intermediate steps of calculating the mean channel depth. **Left to right: (a)** Raw image – **(b)** Segmentation of upper surface – **(c)** Segmentation of channel layer – **(d)** Erosion of (b) – **(e)** Erosion of (c).

results in two or three segments depending on the present number of different layers.

Secondly, in order to remove unwanted areas, which are likely to contain burrs as well as measurement artefacts, morphological erosion is applied to the different segments. Otherwise, these areas would have a negative influence on the calculation and would distort the achieved results. Also small overlapping errors that may be caused by a possibly insufficient registration accuracy are eliminated.

Finally, the mean values r_i and the variances σ_i^2 of all regions in the sensed image, which correspond to the eroded segments derived from the reference image, are calculated. Thus, the mean channel depths d_i are calculated as the absolute difference between the mean value of the eroded upper surface and the mean values of the respective channel layers.

3.2 Identification of Burrs

The recognition of high burrs is realized by the application of several image processing techniques. The algorithm basically consists of three processing steps. The results of the subsequent steps are shown in Fig. 3.

In an initial step, regions have to be identified that are likely to contain burrs. Thus, regions near channel boundaries have to be selected. In contrast, regions on filter columns are not of interest. In order to remove them from analysis, a combination of Otsu segmentation, morphological erosion and region-growing segmentation is employed. The first segmentation step identifies the upper surface, which also contains filter columns. By choosing an appropriate size of the structure element, the applied morphological erosion entirely removes the pillars. As this erosion also moves the channel boundaries, the latter are reconstructed by a subsequent region-growing segmentation with the erosion result as seed points. After this "opening by reconstruction" procedure, the full upper surface without filter columns is available.

Secondly, in order to isolate regions that are likely to contain burrs, a morphological gradient (difference of dilation and erosion) is applied to the segmented upper surface. As a result, the potential burr regions are isolated. Dilation is applied to discard the effects of small misalignments caused by inaccuracies of the registration process.

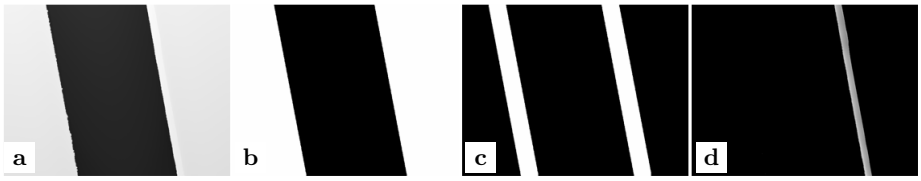

Fig. 3. Results of essential steps in the identification of high burrs. **Left to right: (a)** Raw image – **(b)** Segmentation of the upper surface – **(c)** Morphological gradient – **(d)** Identified burr.

Finally, in order to find high burrs, the identified regions are examined. Burr is signalled at those locations i where the measured height value z_i exceeds the average level $\bar{r}$ of the upper surface by more than a predefined threshold t, i.e. where $|\bar{r} - z| > t$. Burr locations are then collected into connected sets, and aggregated information on these burr regions is reported. This comprises the number of regions, the highest value of each region, the position of the burrs and statistics about sizes and ellipsoidal diameters.

3.3 Calculation of Transcription Accuracy

The algorithm for determining the transcription of all filter columns basically consists of four steps. The results of the steps are presented in Fig. 4.

First, the upper surface is segmented by the Otsu method. In order to identify the single filter columns on the entire upper surface, the surface is divided into its connected components by a morphological labeling step. All connected components are classified into filter columns or non-channel regions. This decision can simply be made based on the sizes of the identified objects. Note that the segmentation procedure is performed on the reference data so that defects of pillars or in channels will not introduce erroneous splitting or joining of segments.

To suppress influence from burrs in near-edge areas and measurement artifacts, all objects identified before are reduced in size by erosion.

Finally, a transcription parameter is calculated for each filter column. This involves the determination of the average value $\bar{r}_i$ of the overlapping regions between the eroded objects (columns) and the template image as well as the calculation of the average value of the upper surface $\bar{r}_0$. Thus, the transcription parameters are the height differences d_i between those respective values,

$$d_i = |\bar{r}_0 - \bar{r}_i| \,, \quad i = 1, \ldots, n \,. \tag{5}$$

3.4 Detection of Defective Regions

The algorithm is divided into three main steps: exclusion of biasing areas, detection of deviations and characterization of the detected deviations. The results of the steps are depicted in Fig. 5.

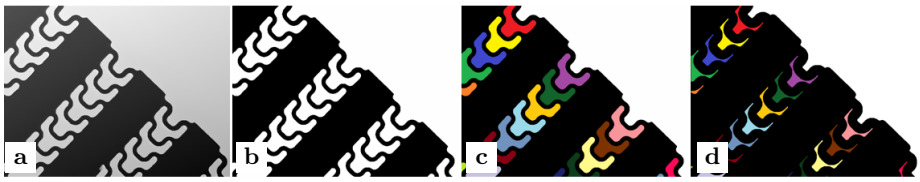

Fig. 4. Results of individual processing steps for calculating the transcription accuracy of all filter columns. **Left to right: (a)** Raw image – **(b)** Segmentation of the upper surface – **(c)** Result of morphological labeling – **(d)** Erosion of the labeled objects.

In a first step, all regions which do not contribute and may have a negative influence on the detection results are excluded from the inspection. As already explained above, those biasing areas are located around the channel boundaries. In order to identify them, the surfaces are segmented by the Otsu method. Similar as in the transcription accuracy analysis, a morphological gradient operation yields an image which contains a segmentation of all areas around the borders.

The second step is to detect all deviations between the reference and the transformed template image. By calculating the difference between the sensed image and the model image as well as excluding the overlapping regions of the result from the first step, it is possible to identify all real deviations. Further application of morphological opening removes the remaining artefacts. This corresponds to a similar approach proposed by Tait et al. [20]. The determination of the structure element's size plays a crucial role in this context. Oversized elements would result in the removal of possible defects, undersized would lead to the detection of small defects, which actually are phantoms. The defects or impurities are then located by applying labeling. At this point the defects are detected as well as labeled and can be characterized.

The last step aims at characterizing the individual defects and reporting information about them. For each defect, its ellipsoidal diameter and size are determined. Aggregating over all defects, statistics of these quantities are calculated, including mean, standard deviation, minimum and maximum. Secondly, information about the location of the defects is gathered. The locations of the defects are determined by several processing steps. At first a distinction between defects on the upper surface outside channels, and defects in channels is made. This is accomplished by inspecting the defects overlapping regions in the reference image and the corresponding intensity values in the model. Additionally, defects within channels are classified into defects within a filter structure, outside but near to a filter structure, or remote from all filter structures. This is accomplished by calculating Euclidean distances between a given defects and the nearest filter columns. If the distances of two or more columns are beneath a given threshold, the defect is located in a filter structure and has the potential to block the structure. If only one filter column is found in the proximity, the defect lies near the filter structure but not within it. Finally, if the number of

Fig. 5. Results of the main processing steps for defect detection. **Left to right: (a)** Raw image – **(b)** Morphological gradient – **(c)** Difference of model and acquired image – **(d)** Opening of (c) – **(e)** Chip image with detected defects overlaid in white (originally, defects are shown in color).

nearby filter columns is equal to zero, the defect lies completely outside the filter structure.

4 Experimental Validation

4.1 Comparison with Manual Inspection

A set of 42 test images were selected to calculate the defined quality parameters. In order to draw a comparison with manual inspection, the manually achieved results were gathered. Unfortunately, it turned out that transcription parameters could not be compared since they showed an excessive operator dependency in manual measurements. Nevertheless, channel depths and burrs could be compared. Results are shown in Fig. 6.

On average there is a difference of $(0.2 \pm 0.15)\,\mu\text{m}$ as far as channel depths are concerned. This deviation is not significant. However, the surface-based calculation of the channel depth is not only highly objective but also reflects the real channel depth of the whole channel depicted in the acquired image.

Surprisingly, there is no correlation between the automatically and the manually determined burrs. From the results in Fig. 6 it is evident that burr heights derived in the automatic procedure are systematically lower than the manually gauged burrs. Part of a possible explanation for this might be the definition of the burr itself. Burrs are raised edges which exceed the normal part geometry and occur at channel edges. Contrary to this definition, no distinction between edges on the filter columns and channel edges is made in the manual gauging process. Moreover, operators doing manual measurements tend to gauge burrs against the surface level in the vicinity of the burr region, which may involve a systematic underestimation of this surface level as compared to the globally adjusted surface level of the automatic procedure.

4.2 Defect Detection

In order to illustrate the localization capabilities of defect detection, the identified deviations were investigated. A set of 50 test images was used for this purpose. Tab. 4.2 shows the localization results. An overall number of 130 defects was detected by the system. At first, the defects were localized as either

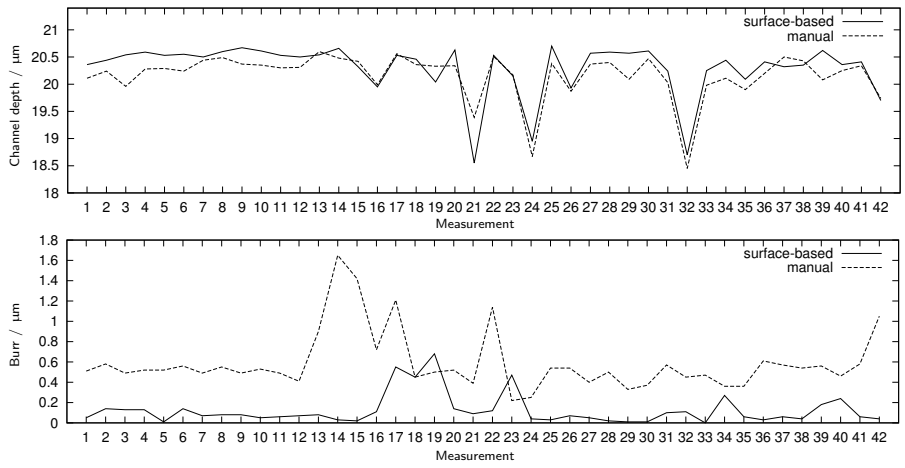

Fig. 6. Top to bottom: (a) Comparison of channel depths – **(b)** Comparison of burrs.

being on the upper surface or within the channel. Altogether, 92 defects were classified as channel defects. The remaining 38 defects were categorized as being located on the upper surface. In addition, the 92 channel defects were classified into three groups: in the filter structure, near the filter structure and outside the filter structure. The system categorized 50 defects as being in the filter structure, 23 defects near the filter structure and 19 as being completely outside the filter. Additionally, the identified defects were manually inspected in order to check the reliability of the system. The classification was done independently from the automated localization. The decision between channel defects and surface defects completely matched with the automated inspection. However, results of the second classification scheme slightly differed between manual investigation and automated inspection. A total number of 54 defects were considered to be in the filter, 20 near the filter and 18 completely outside the filter structure. These small differences may indicate that the parameters for defect localization were still not optimally adapted. Further work has to be done on fine tuning of the parameters.

Table 1. Comparison of manual and automated localization of 130 detected defects.

Localization	Number of defects	
	Automated	Manual
On Surface	38	38
In Channel	92	92
– In Filter	50	54
– Near Filter	23	20
– Outside Filter	19	18

5 Conclusion

We have demonstrated a system for automated quality control of microfluidic chips. The system is capable of both the calculation of different quality characteristics and detection as well as localization of defects. Image registration is used to localize the region of interest and establish independence of rotation and translation. Morphological image processing techniques play a crucial role in the analysis step.

Experimental comparison with manual inspection demonstrated the advantages of the system. The benefit is not only that the demand for human workforce for quality inspection is reduced but also the reproducibility and reliability of so computed quality parameters is higher due to the elimination of the subjective manual gauging. The removal of the human influence leads to an objective evaluation method.

Further work is necessary to raise the performance of the developed system, primarily by more efficient implementation of critical parts, and overall code optimization. Ongoing work focuses on revising the parameters and criteria in the quality inspection. Besides introducing new quality criteria, defect detection needs to be made more specific. For example, shape defects should be distinguished from surface defects. Shape irregularities may result in the jamming of filter structures, thus interfering with the chip's functionality. In contrast, surface defects in uncritical areas may be completely irrelevant. Considerably more work will be needed to develop classification capabilities. Given the determined quality parameters and the number, size as well as location of the detected defects, a classification system will be able to support the operators in deciding whether the chip should be accepted or rejected.

We expect that the further development of the presented system will even strengthen its benefit in terms of objectivity and reliability, and turn it into a powerful tool in routine quality inspection.

References

1. V. Asha, N. Bhajantri, and P. Nagabhushan. GLCM-based chi-square histogram distance for automatic detection of defects on patterned textures. *International Journal of Computational Vision and Robotics,* **2**(4):302–313 (2011)
2. Y.-C. Chiou and Y.-K. Zhang. An edge-based registration method for locating defects on PCB films. In H. R. Arabnia, ed., *Proc. of the 2006 International Conference on Image Processing, Computer Vision, and Pattern Recognition, Las Vegas, Nevada, USA, June 26–29, 2006, Vol. 1*, CSREA Press, 209–215 (2006)
3. R. Duda, P. Hart, and D. Stork. *Pattern Classification.* 2nd edn. Wiley, New York (2001)
4. H. Elbehiery, A. Hefnawy, and M. Elewa. Surface defects detection for ceramic tiles using image processing and morphological techniques. *World Academy of Science, Engineering and Technology,* **5**:158–162 (2005)
5. A. Goshtasby. *Image Registration: Principles, Tools and Methods.* Springer, New York (2012)

6. J. Goutsias and H. Heijmans. Fundamenta morphologicae mathematicae. *Fundamenta Informaticae,* **41**:1–31 (2000)
7. D. Eberly. *Least Squares Fitting of Data.* `http://www.geometrictools.com,` last visited 2012-12-01
8. I. Ibrahim, Z. Ibrahim, K. Khalil, M.M. Mokji, S.A.R.S. Abu Bakar, N. Mokhtar, and W.K.W. Ahmad. An improved defect classification algorithm for six printing defects and its implementation on real printed circuit board images. *International Journal of Innovative Computing, Information and Control,* 8(5(A)):3239–3250 (2-12)
9. F. Leta, F. Feliciano, and F. Martins. Computer vision system for printed circuit board inspection. *ABCM Symposium Series in Mechatronics,* Vol. 3, 623–632 (2008)
10. S. Li. *Markov Random Field Modeling in Image Analysis.* Springer, London (2001)
11. H. Lin, Y. Chiu, and S. Hsu. A visual inspection system for quality control of optical lenses. *International Journal of the Physical Sciences,* **6**(11):2701–2709 (2011)
12. B. Mandelbrot. *The Fractal Geometry of Nature.* W.H. Freeman, New York (1983)
13. J. Maintz and M. Viergever. A survey of medical image registration. *Medical Image Analysis,* **2**:1–36 (1998)
14. A. Mital, M. Govindaraju and B. Subramani. A comparison between manual and hybrid methods in parts inspection. *Integrated Manufacturing Systems,* **9**:344–349 (1998)
15. M. Moganti, F. Ercal, C.H. Dagli and S. Tsunekawa. Automatic PCB inspection algorithms: a survey. *Computer Vision and Image Understanding,* **63**:287–313 (1996)
16. H. Ng. Automatic thresholding for defect detection. *Pattern Recognition Letters,* **27**:1644–1649 (2006)
17. I. Novak and Z. Hocenski. Texture feature extraction for a visual inspection of ceramic tiles. *Proceedings of ISIE,* **3**:1279–1283 (2005)
18. N. Otsu. A threshold selection method from gray-level histograms. *IEEE Transactions on Systems, Man and Cybernetics,* **9**(1):62–66 (1979)
19. F. Shih. *Image Processing and Pattern Recognition.* Wiley, New York (2010)
20. R. Tait, G. Schaefer, and L. Nolle. Automated visual inspection using a distributed blackboard architecture. *International Journal of Simulation, Man and Cybernetics,* **7**(3):12–20 (2006)
21. D. Tsai, C. Lin, and K. Huang. Defect detection in coloured texture surfaces using Gabor filters. *Imaging Science Journal,* **53**(1):27–37 (2005)
22. F. Vilnrotter, R. Nevatia, and K. Price. Structural analysis of natural textures. *IEEE Transactions on Pattern Analysis and Machine Intelligence,* **8**:76–89 (1986)
23. K. Wiltschi, A. Pinz, and T. Lindeberg. An automatic assessment scheme for steel quality inspection. *Machine Vision and Applications,* 12:113–128 (2000)
24. X. Xie. A review of recent advances in surface defect detection using texture analysis techniques. *Electronic Letters on Computer Vision and Image Analysis,* **7**(3):1–22 (2008)
25. X. Xie and M. Mirmehdi. Texture exemplars for defect detection on random textures. *Proc. International Conference on Advances in Pattern Recognition,* 404–413 (2005)
26. H. Zheng, L. Kong and S. Nahavandi. Automatic inspection of metallic surface defects using genetic algorithms. *Journal of Materials Processing Technology,* **5**:158–162 (2002)
27. B. Zitova and J. Flusser. Image registration methods: a survey. *Image and Vision Computing,* **21**:977–1000 (2003)